Research on Chemical Intermediates (2019) 45:1357–1379
https://doi.org/10.1007/s11164-018-3683-7

Structural, vibrational and thermal properties of a new inorganic compound: $Tl_{0.92}(NH_4)_{0.08}(SO_4)_{0.65}(SeO_4)_{0.35}Te(OH)_6$

Atef Elferjani[1] · Santiago Garcia-Granda[2] · Mohamed Dammak[1]

Received: 14 September 2018 / Accepted: 20 November 2018 / Published online: 27 November 2018

Abstract

A new compound thallium ammonium sulfate selenate tellurate: $Tl_{0.92}(NH_4)_{0.08}(SO_4)_{0.65}(SeO_4)_{0.35}Te(OH)_6$ (TlNSSeTe) has been synthesized by slow evaporation at room temperature to specify its phase transition temperatures. X-ray diffractometry data revealed crystallization in the monoclinic system with a $P2_1/c$ space group with these parameters: $a = 12.336(2)$ Å, $b = 7.2038(14)$ Å, $c = 12.017(2)$ Å et $\beta = 110.631(10)°$, $V = 999.4(3)$ Å^3 and $Z = 4$. Three coexisting anions (TeO_6^{6-}, SO_4^{2-} and SeO_4^{2-}) are the main characteristics of these atomic arrangements in the unit cell, related by O–H…O and N–H…O bonds building up the crystal. The cations Tl^+ and NH_4^+ lie at the same positions between these polyhedra. The new synthesized compound has been characterized by using the differential scanning calorimetry (DSC), thermal analysis [differential thermogravimetric analysis (TG), as well as thermodifference analysis (DTA)], FT-IR and Raman spectroscopy techniques. The DSC results demonstrated phase transitions at 384 K, 465 K and 472 K. DTA and TG proved that decomposition takes place in three steps. The vibrational spectroscopy study at room temperature unveiled not only the occurrence and the independence of anionic and cationic groups, but also the importance of the hydrogen bonds.

Keywords Inorganic solid solution · Hydrogen bonds · Anionic groups · Phase transition temperatures

✉ Atef Elferjani
elferjani.atef@yahoo.fr

[1] Laboratory of Inorganic Chemistry, LR 17ES07, University of Sfax, B. P. 1171, 3000 Sfax, Tunisia

[2] Department of Physical and Analytical Chemistry, University Oviedo-CINN, 33006 Oviedo, Spain

Introduction

In recent years, inorganic open-framework compounds based on tellurium oxides have attracted great interest because of their fascinating structural diversities and their various potential applications such as cathode compounds and physics properties [1, 2]. Tellurites are particularly rich for a variety of reasons, including variable coordination numbers, the presence of a stereochemically active lone pair of electrons and the large variability in the coordination environments of the tellurite anion play important roles in the crystalline architecture of this family of materials [3–5]. Furthermore, the combination of tellurite with sulfate in one compound enables novel structures with the potential for creating multifunctional materials [1–3, 6, 7].

In the earlier studies, much work has already been carried out on the telluric acid based materials synthesis, addressing of the interesting physical and chemical properties [8–10]. Inorganic tellurates compounds have attracted much attention in the past several decades, because of their various potential applications such as energy storage devices, electrochemical reactors, multilayer capacitors, solid-state batteries and microelectronic components [11, 12]. Indeed, telluric acid has sparked the interest of scientists due to its role in forming stable adducts to some varieties of organic and inorganic materials of considerable significance by acting as both donor and acceptor of hydrogen bonds [13, 18]. Moreover, multiple authors have demonstrated that certain added materials with selenic and sulfuric acid are extremely interesting for their structural phase transitions, as well as their associated physical properties, such as ferroelectricity, dielectric relaxation, especially a phase transition into a state characterized with a high protonic conductivity [8–10, 17, 18].

The interest in these compounds is due to the presence of different anionic groups (SO_4^{2-}, SeO_4^{2-} and TeO_6^{6-}) in the same unit cell, which can favor a variety of load centers as well as the presence of H^+ protons and the specific features of hydrogen bonds formed in the structure of these crystals. Recently, numerous research works have addressed the characterization of inorganic solid acid materials such as those with the general formula $M_2AO_4Te(OH)_6$ (where M is a monovalent cation: Na, K, NH_4, Tl, Rb and Cs, $A = S$, Se and P) [13–18] and $(NH_4)_{2x}M_{2-2x}SO_4Te(OH)_6$ (M = Rb, Na, K, Cs) [19–21]. In fact, these compounds exhibit structures related to the co-occurrence in the same crystal of independent anions linked via hydrogen bonds and the specific structural arrangement of the polyhedra, which stem from structural dielectric transitions. Several interesting physical properties characterize these inorganic materials such as ferroelectricity, ferroelasticity and ionic-protonic conduction [13–18]. Yet, in the particular case of sulfate selenate tellurates, various works have investigated this family in depth so as to synthesize and explore new materials by modifying the cationic or anionic groups to seek compounds with better structural, physical and chemical properties, for the sake of new uses [22–25].

In this context, the impact of anionic substitution on the structural parameters has been examined. For instance, thallium sulfate selenate tellurate

$Tl_2(SO_4)_{0.61}(SeO_4)_{0.39}Te(OH)_6$ (TlSSeTe), ammonium sulfate selenate tellurate $(NH_4)_2(SO_4)_{0.73}(SeO_4)_{0.27}Te(OH)_6$ (NSSeTe), and ammonium selenate tellurate $(NH_4)_2(SeO_4)Te(OH)_6$ (NSeTe) are recognized by centrosymmetry and crystallization in the monoclinic system with $P2_1/c$ space group [8, 22, 23], whereas the pure compound $Tl_2(SeO_4)Te(OH)_6$ (TlSeTe) displays the space group P21/a [26].

Indeed, NSSeTe exhibits three phase transitions noticed in the DSC curve at 398, 430 and 450 K, which is proved through X-ray powder diffraction at different temperatures [23]. In addition, the original compound TlSeTe is characterized by successive phase transitions at 373, 395 and 437 K, respectively [26]. These are structural transitions associated with specific physical properties, including superionic-protonic conduction and ferroelectricity, which refers basically to the H^+ ions motion throughout the hydrogen bonds [11, 13, 18, 23–25].

In order to improve these features and visualize the effect of the presence of the sulfate and the selenate groups on the structural properties and lattice parameters, we undertook the cationic substitution of the thallium by the ammonium, and the anionic substitution of the sulfate group by the selenate group. Theses substitutions, as well as the presence of a hydrogen atom in this ionic group helped differentiate between this new sulfate selenate tellurate and other previously studied ones and gave new insights into the new compound that is based on tellurate. Therefore, it is highly interesting to make and study the new thallium ammonium sulfate selente tellurate mixed solution.

Our research aims to identify the synthesis conditions and features of the new mixed crystal $Tl_{0.92}(NH_4)_{0.08}(SO_4)_{0.65}(SeO_4)_{0.35}Te(OH)_6$ (TlNSSeTe) based on the structural characterization by XRD and vibrational studies, phase transitions through differential scanning calorimetry (DSC), thermodifference analysis (DTA), and the decomposition of the material via differential thermogravimetric analysis (TG) analysis.

Experimental details

Chemical preparation

The single crystals of the thallium ammonium sulfate selenate tellurate $Tl_{0.92}(NH_4)_{0.08}(SO_4)_{0.65}(SeO_4)_{0.35}Te(OH)_6$ (TlNSSeTe) were obtained by slow evaporation at room temperature from a mixture of telluric acid H_6TeO_6, ammonium carbonate $(NH_4)_2CO_3$, thallium carbonate Tl_2CO_3, sulfuric acid H_2SO_4 and selenic acid H_2SeO_4 repeated in a stoechiometric ratio with the following reaction:

$$(1-y)\,Tl_2CO_3 + y\,(NH_4)_2CO_3 + (1-x)\,(H_2SO_4) + x\,H_2SeO_4 + H_6TeO_6 \rightarrow Tl_{2-2y}(NH_4)_{2y}(SO_4)_{1-x}(SeO_4)_xTe(OH)_6 + CO_2 + H_2O \quad (1)$$

A fortnight after, transparent and colorless single crystals of $Tl_{0.92}(NH_4)_{0.08}(SO_4)_{0.65}(SeO_4)_{0.35}Te(OH)_6$ were obtained. Certain recrystallizations were essential to obtain single crystals convenient for the X-ray study.

The formula of the title compound was determined by chemical analysis and proved by the improvement of the crystal structure. The elementary chemical analyses that are used for the determination of the formula are inductively coupled plasma mass spectrometry (ICP-MS) method for the percentages of tellurium, selenium and thallium, and the percentage of sulfur is determined by complexometry, while the Kjeldahl for the percentage of nitrogen. All the values obtained are summarized in Table 1.

Density was evaluated using flotation in CCl_4 at room temperature. The average value of density, $D_m = 4.78(5)$ g cm^{-3} was confirmed to be in good line with the calculated one $D_{cal} = 4.93(5)$ g cm^{-3}.

Diffraction data collection and refinement

A suitable single crystal of TlNSSeTe was chosen for the structure determination and refinement. It was selected under a polarizing microscope and was mounted on a glass fiber. For the crystal structure determination, single crystal X-ray diffraction was mounted on a Enraf–Nonius Kappa CCD diffractometer equipped with graphite-monochromated Mo Kα radiation ($\lambda = 0.71073$ Å) [27]. Data were collected at room temperature. We determined unit cell dimensions through the indexation of diffraction markings depicted by Bruker–Nonius X8-APEX2 CCD area-detector diffractometer through APEX2 program [28].

A total of 3412 reflections were determined, 1344 of which had an intensity of $I > 2\sigma(I)$. The crystal structure was successfully developed in the monoclinic system at a $P2_1/c$ centrosymmetric space group. The structure was solved with the crystallographic CRYSTALS program [29], and the structural figures were drawn using the DIAMOND program [30]. The Te, Tl and N atom positions were refined by Patterson method and the O atom positions were established from difference Fourier maps, while all hydrogen atoms were geometrically placed. When all atoms were anisotropically refined, the final cycle of refinement leads to the final value of the discrepancy factors R and wR which were found to be 0.059 and 0.072, respectively.

The final atomic positions and the Ueq parameters for the new mixed compound are displayed in Tables 2 and 3, respectively. The main interatomic distances (Å) and bond angles (°) for our solid solution are exhibited in Tables 4 and 5.

Thermal behavior measurements

The DSC measurement was carried out with a NETZSCH apparatus (Model 204 Phoenix) for temperatures ranging from 350 to 600 K, using a constant heating

Table 1 Results of the chemical analyses for $Tl_{0.92}(NH_4)_{0.08}(SO_4)_{0.65}(SeO_4)_{0.35}Te(OH)_6$

Analyses result	Te (%)	Tl (%)	N (%)	S (%)	Se (%)
Experimental	17.11	25.27	0.10	2.72	3.65
Theoretical	17.19	25.33	0.15	2.80	3.72

Table 2 Main crystallographic feature X-ray diffraction data parameters results of $Tl_{0.92}(NH_4)_{0.08}(SO_4)_{0.65}(SeO_4)_{0.35}Te(OH)_6$

Formula	$Tl_{0.92}(NH_4)_{0.08}(SO_4)_{0.65}(SeO_4)_{0.35}.Te(OH)_6$
Formula weight ($gmol^{-1}$)	742.05
T (K)	293
Crystal system	Monoclinic
Space group	$P2_1/c$
Unit cell dimensions	$a = 12.336(2)$ Å
	$b = 7.2038(14)$ Å
	$c = 12.017(2)$ Å
	$\beta = 110.631(10)°$
	$V = 999.4(3)$ Å^3
Z	4
Dx (g cm^{-3})	4.931
θ range for data collection (°)	1.8-25.4
μ (mm^{-1})	3.80
hkl range	$-14 \le h \le 14$
	$-8 \le k \le 0$
	$-14 \le 1 \le 14$
Data collection instrument	Kappa CCD
Wavelength (Å)	0.71073
Measured reflections	3412
Observed reflections $I > 3\sigma(I)$	1344
Parameters refined	95
R indices	$R = 0.059$ and $R_w = 0.072$
Goodness-of-fit on (F^2)	1.03
Highest peak/deepest hole (eÅ^3)	$-4.49 < \Delta\rho < 4.63$
$w = 1/[\sigma^2 (Fo^2) + (0.0800P)^2 + 0P]$ where $P = (Fo^2 + 2Fc^2)/3$	
CCDC deposition number	1,837,068

rate of 5 K min^{-1}. A sample of 6.914 mg was placed inside an aluminum crucible in nitrogen atmosphere.

Thermodifferential and thermogravimetric measurements (TG–DTA) of the title compound were performed with Mettler Toledo model TGA851ELF and Setaram model Setsys Evolution 16 thermobalances. Samples were placed inside uncovered an aluminum crucible. The mass of samples used in TG and DTA measurements were 14.068 mg. They were heated from 300 to 1100 K and at heating rate of 5 K/min. In the TG test, a Pfeiffer Vacuum ThermoStarTM GSD301 T mass spectrometer was used to characterize the evacuated vapors.

Table 3 Atomic coordinates and equivalent thermal parameters

Atoms	*x*	*y*	*z*	U_{eq}	Occupation
Te1	1.0000	0.0000	1.0000	0.0146 (5)	1.0000
Te2	0.5000	−0.5000	1.0000	0.0148 (5)	1.0000
Tl1	0.64662 (3)	−0.03503 (3)	0.89464 (3)	0.0175 (5)	0.91957 (4)
N1	0.64662 (3)	−0.03503 (3)	0.89464 (3)	0.0175(5)	0.07957 (4)
Tl2	0.15425 (4)	0.50164 (4)	0.85564 (4)	0.0179 (5)	0.92002 (3)
N2	0.15425 (4)	0.50164 (4)	0.85564 (4)	0.0179 (5)	0.08002 (3)
Se1	0.74983 (4)	−0.49105 (4)	0.74420 (4)	0.0365 (5)	0.65230 (4)
S1	0.74983 (4)	−0.49105 (4)	0.74420 (4)	0.0365 (5)	0.35230 (4)
O1	0.8607 (6)	0.1150 (8)	0.8959 (7)	0.0240 (5)	1.0000
O2	0.9032 (7)	−0.2057 (8)	1.0073 (7)	0.0310 (5)	1.0000
O3	0.9832 (7)	0.1074 (8)	1.1369 (7)	0.0318 (5)	1.0000
O4	0.6261 (7)	−0.4312 (8)	0.9516 (7)	0.0266 (5)	1.0000
O5	0.3875 (7)	−0.4228 (8)	0.8504 (7)	0.0211 (5)	1.0000
O6	0.4940 (7)	−0.7442 (8)	0.9355 (7)	0.0234 (5)	1.0000
O7	0.8567 (7)	−0.5090 (8)	0.8603 (8)	0.0275 (5)	1.0000
O8	0.7214 (7)	−0.2838 (8)	0.7221 (7)	0.0288 (5)	1.0000
O9	0.7727 (7)	−0.5790 (8)	0.6388 (7)	0.0269 (5)	1.0000
O10	0.6445 (7)	−0.5877 (8)	0.7558 (7)	0.0265 (5)	1.0000
H1	0.8162	0.1385	0.9444	0.0285	1.0000
H2	0.8699	−0.2014	1.0671	0.0432	1.0000
H3	0.9993	0.1840	1.2054	0.0419	1.0000
H4	0.6947	−0.4690	1.0152	0.0303	1.000
H5	0.3552	−0.3004	0.8431	0.0313	1.0000
H6	0.4195	−0.7952	0.8967	0.0296	1.0000
H7	0.6716	0.0889	0.8913	0.0210	1.0000
H8	0.6805	−0.0809	0.9735	0.0210	1.0000
H9	0.5646	−0.0376	0.8715	0.0210	1.0000
H10	0.6698	−0.1107	0.8422	0.0210	1.0000
H11	0.1718	0.6277	0.8462	0.0215	1.0000
H12	0.1547	0.4828	0.9340	0.0215	1.0000
H13	0.0798	0.4723	0.7999	0.0215	1.0000
H14	0.2107	0.4237	0.8424	0.0215	1.0000

$U_{eq} = 1/3 \sum_i \sum_j U_{ij} a_i^* a_j^* a_i a_j$

Spectroscopic measurements

The infrared absorption measurements were performed with a Jasco-FT-IR-420 spectrophotometer. Each sample was mixed with high-purity KBr and then pressed into a disk. The spectra were recorded at room temperature for KBr disks in the spectral range between 400 and 4000 cm^{-1}.

Table 4 Anisotropic displacement parameters of $Tl_{0.92}(NH_4)_{0.08}(SO_4)_{0.65}(SeO_4)_{0.35}Te(OH)_6$ material

Atoms	U^{11}	U^{22}	U^{33}	U^{12}	U^{13}	U^{23}
Te1	0.01849 (4)	0.00668 (4)	0.02166 (4)	0.00145 (4)	0.01078 (4)	0.00164 (4)
Te2	0.02081 (4)	0.00620 (4)	0.02014 (4)	0.00215 (4)	0.01054 (4)	0.00182 (4)
Tl1	0.02307 (3)	0.00800 (3)	0.02307 (3)	−0.00106 (3)	0.01021 (3)	−0.00058 (3)
N1	0.02307 (3)	0.00800 (3)	0.02307 (3)	−0.00106 (3)	0.01021 (3)	−0.00058 (3)
Tl2	0.02129 (4)	0.00869 (4)	0.02359 (4)	0.00096 (4)	0.00775 (4)	0.00192 (4)
N2	0.02129 (4)	0.00869 (4)	0.02359 (4)	0.00096 (4)	0.00775 (4)	0.00192 (4)
Se1	0.03800 (4)	0.02891 (4)	0.04395 (4)	0.00004 (4)	0.01612 (4)	−0.00043 (4)
S1	0.03800 (4)	0.02891 (4)	0.04395 (4)	0.00004 (4)	0.01612 (4)	−0.00043 (4)
O1	0.0166 (4)	0.0263 (8)	0.0314 (6)	0.0046 (4)	0.0112 (6)	0.0088 (7)
O2	0.0225 (5)	0.0239 (7)	0.0466 (8)	−0.0075 (5)	0.0121 (7)	0.0112 (6)
O3	0.0384 (6)	0.0360 (8)	0.0268 (5)	0.0110 (7)	0.0189 (5)	−0.0024 (6)
O4	0.0240 (4)	0.0257 (8)	0.0328 (8)	−0.0094 (7)	0.0135 (5)	0.0016 (7)
O5	0.0259 (5)	0.0094 (7)	0.0236 (5)	−0.0017 (8)	0.0034 (5)	0.0008 (5)
O6	0.0302 (6)	0.0067 (5)	0.0278 (8)	−0.0015 (6)	0.0033 (6)	−0.0025 (5)
O7	0.0352 (5)	0.0079 (8)	0.0424 (6)	−0.0019 (7)	0.0173 (5)	−0.0062 (8)
O8	0.0201 (6)	0.0274 (3)	0.0364 (9)	−0.0045 (5)	0.0068 (8)	−0.0049 (6)
O9	0.0227 (6)	0.0204 (8)	0.0364 (6)	0.0046 (8)	0.0089 (5)	0.0086 (7)
O10	0.0339 (5)	0.0137 (8)	0.0337 (8)	0.0033 (6)	0.0140 (5)	−0.0112 (8)

The anisotropic displacement exponent takes the form: $\exp[-2\pi^2 \sum_i \sum_j Uij\ h_i h_j\ a_i a_j^*]$

Furthermore, the Raman spectroscopy data of polycrystalline samples were recorded at room temperature on a Horiba Labram HR 800 spectrometer using the 632.81 nm exciting light of argon laser. The measurements were performed in the 50–1200 cm^{-1} range, with 3 cm^{-1} resolution.

Results and discussion

Structural properties

The X-ray single-crystal analysis of $Tl_{0.92}(NH_4)_{0.08}(SO_4)_{0.65}(SeO_4)_{0.35}Te(OH)_6$ (TlNSSeTe) reveals that this compound crystallizes at room temperature in monoclinic space group $P2_1/c$, which is also the case for the $(NH_4)_2(SO_4)_{0.73}(SeO_4)_{0.27}Te(OH)_6$ (NSSeTe) structure [23]. We recorded a significant variation in the lattice parameters. Indeed, in our compound (TlNSSeTe), the unit cell data are: $a = 12.336(2)$ Å, $b = 7.2038(14)$ Å, $c = 12.017(2)$ Å, $\beta = 110.631(10)°$, $Z = 4$ and $V = 999.4(3)$ $Å^3$.

However, for the ammonium sulfate selenate tellurate (NSSeTe) structure, the recorded parameters are: $a = 13.7340$ (2) Å, $b = 6.6583$ (1) Å, $c = 11.4582(2)$ Å, $\beta = 106.8270$ (6)°, $Z = 2$ and $V = 1002.93(3)$ $Å^3$ [23]. Meanwhile, the TlSSeTe structure undergoes crystallization in the monoclinic space group $P2_1/a$ with different unit cell parameters, $a = 12.0883(3)$ Å, $b = 7.2207(1)$ Å, $c = 12.3820(2)$ Å,

Table 5 Selected bond lengths (Å) and bond angles (°)

a-Thallium/ammonium groups	
Tl/N(1)–O1 = 2.848 (8)	Tl/N(2)–O3(xi) = 2.836 (7)
Tl/N(1)–O9(iii) = 2.917 (8)	Tl/N(2)–O8(iv) = 2.905 (8)
Tl/N(1)–O5(iv) = 2.939 (8)	Tl/N(2)–O4(vii) = 2.919 (7)
Tl/N(1)–O4 = 2.965 (6)	Tl/N(2)–O2(vii) = 2.926 (7)
Tl/N(1)–O6(v) = 2.970 (7)	Tl/N(2)–O5(v) = 2.949 (8)
Tl/N(1)–O8 = 3.123 (8)	Tl/N(2)–O1(iv) = 3.076 (8)
Tl/N(1)–O2 = 3.215 (8)	Tl/N(2)–O9(viii) = 3.140 (6)
Tl/N(1)–O10(iv) = 3.423 (8)	Tl/N(2)–O3(ix) = 3.304 (7)
Tl/N(1)–O6(ii) = 3.495 (9)	Tl/N(2)–O7(vii) = 3.463 (9)
b-Sulfate/selenate groups	
Se/S–O7 = 1.550 (8)	O7–Se/S–O8 = 107.9 (3)
Se/S–O8 = 1.535 (6)	O7–Se/S–O9 = 111.4 (4)
Se/S–O9 = 1.529 (8)	O8–Se/S–O9 = 110.9 (4)
Se/S–O10 = 1.523 (8)	O7–Se/S–O10 = 111.2 (4)
	O8–Se/S–O10 = 108.1 (4)
	O9–Se/S–O10 = 107.4 (4)
c-Tellurate groups	
Te1–O2(i) = 1.925 (7)	Te2–O5(ii) = 1.926 (7)
Te1–O1(i) = 1.921 (7)	Te2–O6(ii) = 1.914 (6)
Te1–O3(i) = 1.894 (8)	Te2–O4(ii) = 1.908 (8)
Te1–O1 = 1.921 (7)	Te2–O4 = 1.908 (8)
Te1–O2 = 1.925 (7)	Te2–O5 = 1.926 (7)
Te1–O3 = 1.894 (8)	Te2–O6 = 1.914 (6)
O2(i)–Te1–O1(i) = 86.3 (3)	O5ii–Te2–O6ii = 88.6 (3)
O2(i)–Te1–O3(i) = 90.9 (3)	O5ii–Te2–O4ii = 92.1 (3)
O1(i)–Te1–O3(i) = 92.5 (3)	O6ii–Te2–O4ii = 92.0 (3)
O2(i)–Te1–O1 = 93.7 (3)	O5ii–Te2–O4 = 87.9 (3)
O1(i)–Te1–O1 = 180	O6ii–Te2–O4 = 88.0 (3)
O3(i)–Te1–O1 = 87.5 (3)	O4ii–Te2–O4 = 180
O2(i)–Te1–O2 = 180	O5ii–Te2–O5 = 180
O1(i)–Te1–O2 = 93.7 (3)	O6ii–Te2–O5 = 91.4 (3)
O3(i)–Te1–O2 = 89.1 (3)	O4ii–Te2–O5 = 87.9 (3)
O1–Te1–O2 = 86.3 (3)	O4–Te2–O5 = 92.1 (3)
O2(i)–Te1–O3 = 89.1 (3)	O5ii–Te2–O6 = 91.4 (3)
O1(i)–Te1–O3 = 87.5 (3)	O6ii–Te2–O6 = 180
O3(i)–Te1–O3 = 180	O4ii–Te2–O6 = 88.0 (3)
O1–Te1–O3 = 92.5 (3)	O4–Te2–O6 = 92.0 (3)
O2–Te1–O3 = 90.9 (3)	O5–Te2–O6 = 88.6 (3)

Symmetry codes : (i) $-x+2.-y.-z+2$; (ii) $-x+1.-y-1.-z+2$; (iii) $x.-y-1/2.z+1/2$; (iv) $-x+1.y+1/2.-z+3/2$; (v) $x.y+1.z$; (vi) $x-1.-y+1/2.z-1/2$; (vii) $-x+1.-y.-z+2$; (viii) $-x+1.y+3/2.-z+3/2$; (ix) $-x+1.-y+1.-z+2$

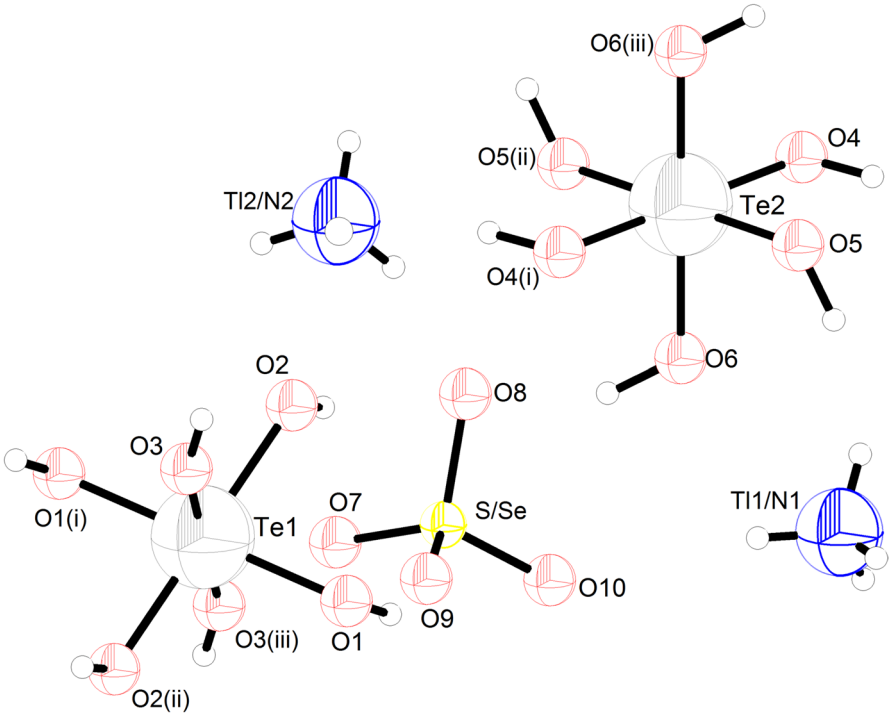

Fig. 1 The asymmetric unit with atom labels and 50% probability displacement ellipsoids for non-H atoms of $Tl_{0.92}(NH_4)_{0.08}(SO_4)_{0.65}(SeO_4)_{0.35}Te(OH)_6$

$\beta = 111.316(1)°$, $Z = 4$ et $V = 1006.84$ (8) Å^3 [22]. The cell volume of TlNSSeTe is different from that of NSSeTe, which may refer to the difference between the cations bulk.

The structure in the studied TlNSSeTe solid solution is not isotype to the base compounds. Indeed, the ammonium sulfate tellurate described by Zilber et al. [15] crystallizes in the monoclinic system with the non-centrosymmetric space group Cc in favor of a ferroelectric phase, and cell parameters: $a = 13.741$ (8) Å, $b = 6.31$ (2) Å, $c = 11.405$ (7) Å, $\beta = 106.75$ (5)°, $Z = 4$, $V = 995$ (2) Å^3. As shown in Fig. 1, the asymmetric unit of the TlNSSeTe is formed by $Te(OH)_6$ octahedra, S/SeO_4 tetrahedra and Tl^+/NH_4^+ cations. The projection of the crystal structure on the ac plane is depicted in Fig. 2.

An examination of the structure indicates clearly three dissimilar anions (SO_4^{2-}, SeO_4^{2-} and TeO_6^{6-} groups) coexisting in the same crystal, related by O–H…O and N–H…O hydrogen bonds that make up the structure of the crystal. In this case, sulfur and selenium atoms are statistically distributed over the same site. This hypothesis is well supported by the IR and Raman data discussed hereafter.

Indeed, the planes of the pure $Te(OH)_6$ octahedra at $x = 0$ and $x = a/2$ alternate with those of the planes of pure S/SeO_4 tetrahedra at $x = a/4$ and $x = 3a/4$. The S and Se atoms occupy the same crystallographic sites. Furthermore, the Tl^+ and

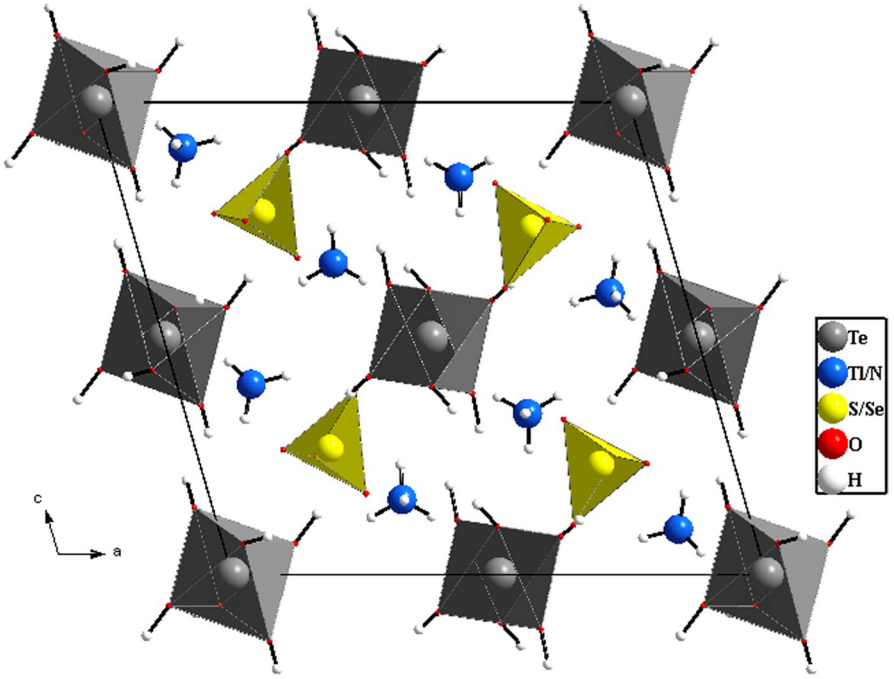

Fig. 2 Projection of crystal structure $Tl_{0.92}(NH_4)_{0.08}(SO_4)_{0.65}(SeO_4)_{0.35}.Te(OH)_6$ on the AC plane

NH_4^+ cations are located between these types of polyhedra. In what follows, the discussion of the new structure refers to TlSSeTe and NSSeTe.

Geometry and environment of TeO_6 groups

In the structure of the new tellurate TlNSSeTe, the oxidation state for Te atom is +VI. It must be noted that the Te^{VI} is coordinated by six atoms of oxygen in a octahedral coordination environment, whereas, in the materials $[M_2Te_4O_{11}]X_2$ (M = Pu, Ce, Zr; X = Cl, Br) a based tellurium oxides, the Te atom has the oxidation state +IV. It is coordinated by three oxygen atoms in the TeO_3 trigonal pyramidal. Furthermore, in Te_3O_8 groups, the central Te^{IV} connects to four oxygen atoms and the other two Te atoms are bonded to three oxygen atoms [4].

In the present structure, the Te atom occupies two special positions. Yet, the Te atom in the NSTe structure occupies only one general position [15]. In each one, an octahedrall coordination is composed of six oxygen atoms (Fig. 3a). As a result, the TlNSSeTe structure presents two types of octahedra $Te(1)O_6$ and $Te(2)O_6$.

As for the octahedral group, the Te–O distances vary from 1.894(8) to 1.926(7) Å and O–Te–O angles from 86.3(3) to 93.7(3). In fact, in the octahedral group, the Te(1)–O distances of the first groups vary from 1.894(8) to 1.925(7) Å with the O–Te(1)–O angle values between 86.3(3)° and 93.7(3)°. However, the scope of distances is from 1.908(8) to 1.926(7) Å with O–Te(2)–O angle values between

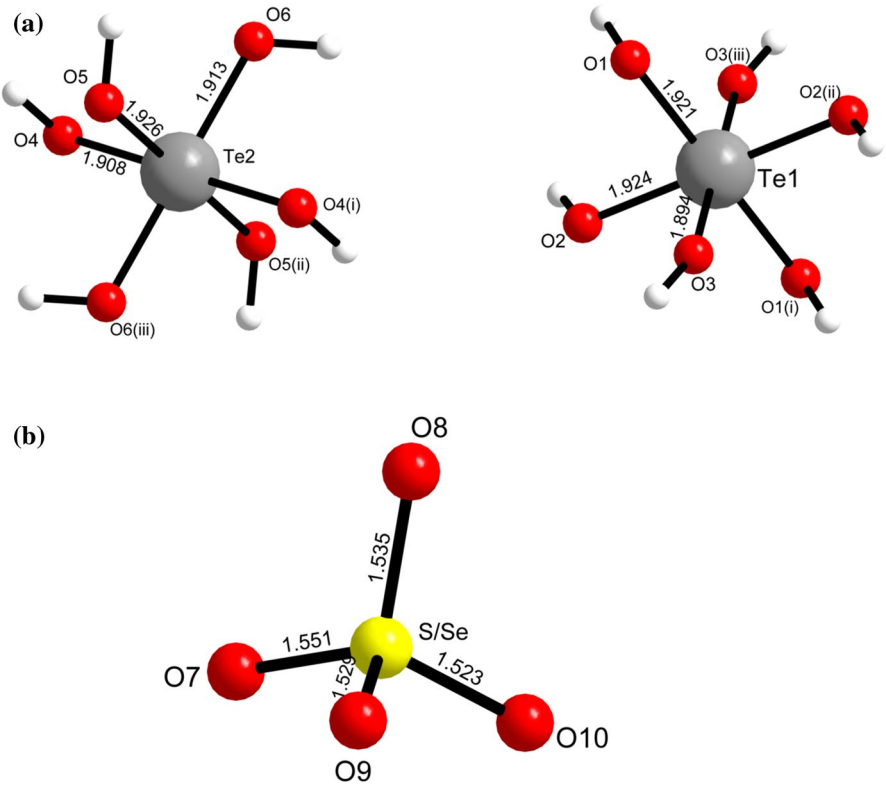

Fig. 3 **a** The environment around the Te atom. **b** The environment around S/Se atoms

87.90(3)° and 91.4(3)° (Table 3), showing that the shape of $Te(2)O_6$ is slightly more distorted than that of $Te(1)O_6$.

Therefore, we infer that these obtained values diverge from those recorded in the preceding studied materials. In fact, in the ammonium sulfate selenate tellurate $(NH_4)_2(SO_4)_{0.73}(SeO_4)_{0.27}Te(OH)_6$ (NSSeTe) structure, the Te–O distances are from 1.908(4) to 1.919(5) Å with O–Te–O angles between 86.6(2)° and 92.1(3)° [23]. On the other side, in the thallium sulfate selenate tellurate $Tl_2(SO_4)_{0.61}(SeO_4)_{0.39}Te(OH)_6$ (TlSSeTe) material, the Te–O distances are between 1.886(10) and 1.979(11) Å. However, the O–Te–O angles vary from 86.2(2)° to 93.8(2)° [22].

As a matter of fact, all these Te–O distances and the O–Te–O angle values prove clearly that the TeO_6 octahedra are less regular in the new material than in the NSSeTe, TlSSeTe compounds. This phenomenon can be the effect of partial cationic substitution.

Moreover, we can observe that these octahedra in the TlNSSeTe structure are highly deformed as compared to $Te(OH)_6$ octahedra in the NSTe original material, where the Te–O distances vary from 1.874(10) to 1.944(9) Å with O–Te–O angles between 76.4(4)° and 92.8(4)° [15].

In fact, the values of both Te–O distances and angular distortion go up when the anionic group volume goes down. This phenomenon can be assigned to the presence of various anionic and cationic entities in this new structure. The presence of TeO_6 group was confirmed using infrared and Raman spectroscopy.

Geometry and environment of S/SeO_4 groups

The structure of TlNSSeTe displays one type of S/SeO_4 tetrahedron. Each S/Se atom center is coordinated by four atoms of oxygen in a tetrahedral coordination environment (Fig. 3b). Actually, in our compound, the sulfur and selenium atoms occupy the same site in respective proportions 65 and 35%.

In NSSeTe solid solution structure, S/Se–O distances vary from 1.481(5) to 1.545(4) Å while O–S/Se–O angles range between 107.0(3)° and 111.3(4)° [23]. The S/Se–O distances vary from 1.528(14) to 1.546(12) Å for TlSSeTe structure [23], whereas, in the mixed TlNSSeTe material, the S/SeO_4, bonds are between 1.523(8) and 1.550(8) Å and the O–S/Se–O angles vary from 107.4(4)° to 111.4(4)°.

It is to be noted that the discrepancy between the present values and those found in the NSSeTe, TlSSeTe compounds is related to the cation radii size, which might be due to the partial cationic substitution.

In previously reported $Ni_3(TeO_3)(SO_4)(OH)_2{\cdot}2H_2O$, the sulfur atoms occupy only one general position, which is coordinated by four oxygen atoms, forming distorted SO_4 tetrahedra. The S–O bond lengths range from 1.467(7) to 1.503(6) Å and the angles of O–S–O from 108.1(2)° to 111.5(4)° [31]. In this case, the tetrahedron of S/SeO_4 is more distorted than that of SO_4 in the tellurite material.

The presence of SO_4^{2-} and SeO_4^{2-} anions was confirmed using infrared and Raman spectroscopy. So, we can deduce that the difference in obtained values compared to previously investigated compounds refers basically to the size of the partial cationic and anionic substitutions.

The lengths and angles of bond for the S/SeO_4 tetrahedra are displayed in Table 5.

The thallium/ammonium cation environment

In the unit cell, the thallium and ammonium atoms in the studied TlNSSeTe solid solution are located on two sites that are sandwiched between the S/SeO_4 tetrahedral and $Te(OH)_6$ octahedral planes. In the original compound $(NH_4)_2SO_4Te(OH)_6$, the NH_4^+ cations do not have the same coordination. In fact, firstly, the ammonium atoms are coordinated by eight and seven oxygen atoms, respectively, with N–O distances varying from 2.271(1) to 3.486(1) Å [15].

Indeed, in the new (TlNSSeTe) crystal structure, nine atoms of oxygen coordinate the Tl(1)/N(1) and Tl(2)/N(2) cations within the mixed structure (TlNSSeTe) as for ammonium sulfate selenate tellurate. Actually, the $Tl(1)^+/N(1)H_4$ environment is composed of two oxygen atoms that belong to $Te(1)O_6$, four oxygen atoms of second octahedral $Te(2)O_6$ and three oxygen atoms that belong to S/SeO_4 tetrahedra (Fig. 4a).

The Tl(1)/N(1)–O distances vary from 2.848(8) to 3.495(9) Å. The environment of $Tl(2)/N(2)H_4$ is composed of four oxygen atoms belonging to $Te(1)O_6$,

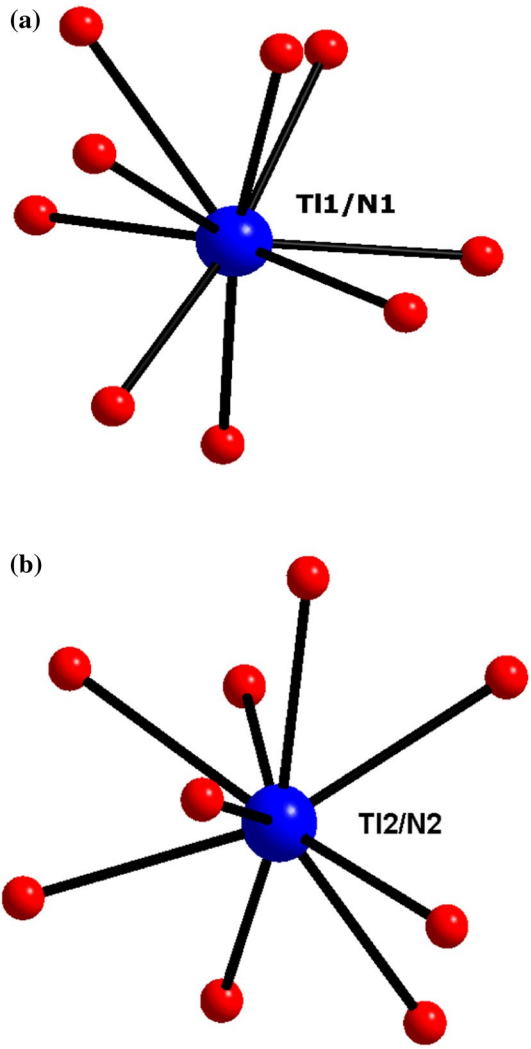

Fig. 4 **a** The coordination of $Tl(1)^{+}/N(1)H_4^{+}$ cations. **b** The coordination of $Tl(2)^{+}/N(2)H_4^{+}$ cations

two oxygen atoms of second octahedral $Te(2)O_6$ and the others belonging to S/SeO_4 tetrahedra (Fig. 4b). Tl(2)/N(2)–O distances vary between 2.836(7) and 3.463(9) Å. Table 5 depicts the thallium/ammonium coordination. As opposed to the thallium sulfate tellurate compound (TlSSeTe), the first Tl(1) atom is coordinated by six oxygen atoms while the second by seven, with distance lengths between 2.842(12) and 3.151(9) Å [22].

Therefore, the high coordination of the thallium/ammonium cations in the studied structure justifies the stability of this new mixed (TlNSSeTe) structure in view of the high interaction between cationic and anionic groups.

The hydrogen bonding

The hydrogen bonds are the most significant intermolecular bonding phenomena in inorganic materials. In fact, they correspond to the linking interactions between hydrogen atoms and negatively charged atoms with (or without) lone pairs [32].

Multiple results of experimental and theoretical studies on hydrogen bonds have been investigated [23, 33, 34]. In the past, investigations conducted on sulfate selenate tellurate compounds turned out to be useful for interpreting the main traits of the hydrogen bond [11].

The stability of the new crystal structure of TlNSSeTe is maintained by two hydrogen bond types On the one hand, the O–H…O hydrogen bond guarantees the association between the S/SeO_4 tetrahedra and the TeO_6 octahedra. On the other hand, the N–H…O ensures the connection between anionic and ammonium groups. Hence, the presence of the O–H…O and N–H…O bonds proves that the studied material displays interesting physical properties [22, 23, 35].

A projection view of the title compound is exhibited in Fig. 5 which reveals the hydrogen bonding in TlNSSeTe. It should be noted that the S/SeO_4 groups are associated with TeO_6 and NH_4 groups via O–H…O and N–H…O bonds. Conversely, the TlKSSeTe compound presents only one type of hydrogen bonds that is ensured by protons from hydroxide groups connecting octahedral and tetrahedral groups [34].

The geometrical features of the network of hydrogen bonds are exhibited in Table 5. We can infer that the hydrogen bonds, depicted in this structure, contribute

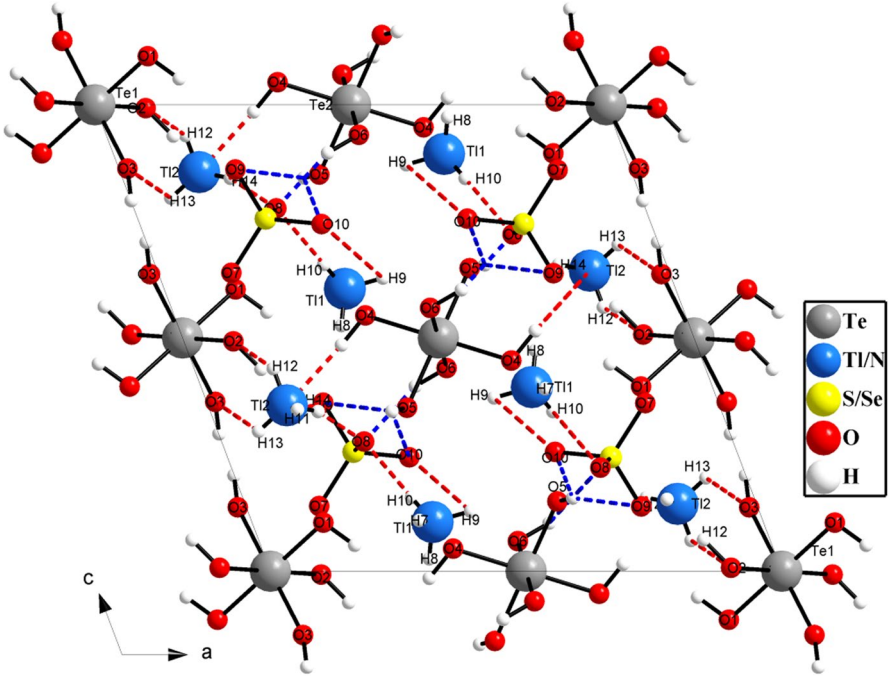

Fig. 5 Projection of the structure $Tl_{0.92}(NH_4)_{0.08}(SO_4)_{0.65}(SeO_4)_{0.35}.Te(OH)_6$ showing the hydrogen bonds

Table 6 Hydrogen-bond and short contact geometry (Å. °)

D–H···A	D–H	H···A	D···A	D–H···A
O4–H4···N2(iii)	0.958	1.975	2.922	169.8 (4)
O5–H5···O9(iv)	0.959	2.307	3.200	154.6 (5)
O5–H5···O10(iv)	0.959	1.940	2.694	133.8 (6)
O6–H6···O8(v)	0.947	1.821	2.680	149.6 (5)
N1–H8···O9(vi)	0.950	2.230	2.913	128.01 (2)
N1–H9···O10(iv)	0.950	2.519	3.426	159.6 (2)
N1–H10···O8	0.950	2.166	3.116	179.6 (2)
N2–H11···O9(vii)	0.950	2.208	3.147	169.2 (2)
N2–H12···O2(iii)	0.950	2.312	2.929	122.1 (2)
N2–H12···O7(iii)	0.950	2.531	3.464	167.10 (1)
N2–H13···O3(viii)	0.950	1.986	2.841	148.8 (3)
N2–H14···O8(iv)	0.950	1.999	2.910	159.8 (2)

*S*ymmetry codes:(iii) $-x+1.-y.-z+2$;
(iv) $-x+1.y+1/2.-z+3/2$; (v) $-x+1.y-1/2.-z+3/2$;
(vi) $x.-y-1/2.z+1/2$; (vii) $-x+1.y+3/2.-z+3/2$;
(viii) $x-1.-y+1/2.z-1/2$

to the formation of chains parallel to $\vec{b}$ direction (Fig. 5). In fact, the O…O distances are between 2.680 and 3.200 Å. In this compound, the O–H distances vary from 1.821 to 2.307 Å with O–H…O angles ranging between 122.1(2)° and 179.6(2)°. The hydrogen atoms are geometrically located within this structure.

Based the NOVAK criterion, our compound's crystal structure displays two types of hydrogen bonds, i.e., strong bonds for O…O distances smaller than 2.7 Å and weaker bonds otherwise [36]. All these findings are reported in Table 6.

These values are slightly higher than those found in TlKSSeTe structure. Therefore, the insertion of Tl^+ with NH_4^+ in TlKSSeTe can decrease the stability of this new structure. Along with the O–H…O hydrogen bonds, the structure of this mixed material is stabilized by N–H…O hydrogen bonding. Hydrogen atoms belonging to the first and the second type of NH_4^+ group participate in the formation of this type of hydrogen bonds. In fact, the obtained O–H distances vary from 1.975 to 2.312 and N–H···O angles are between 122.8(2)° and 179.6(2)°.

In the crystal structure of (TlNSSeTe), the presence of the two types of hydrogen bonds, and all O…O, O…H values are at the origin of very interesting physical properties such as protonic conduction at high temperature.

Thermal analysis

Calorimetry study

In order to determine the expected phase transition at high temperature, DSC measurements of TlNSSeTe samples were carried out from 350 to 600 K at a heating rate

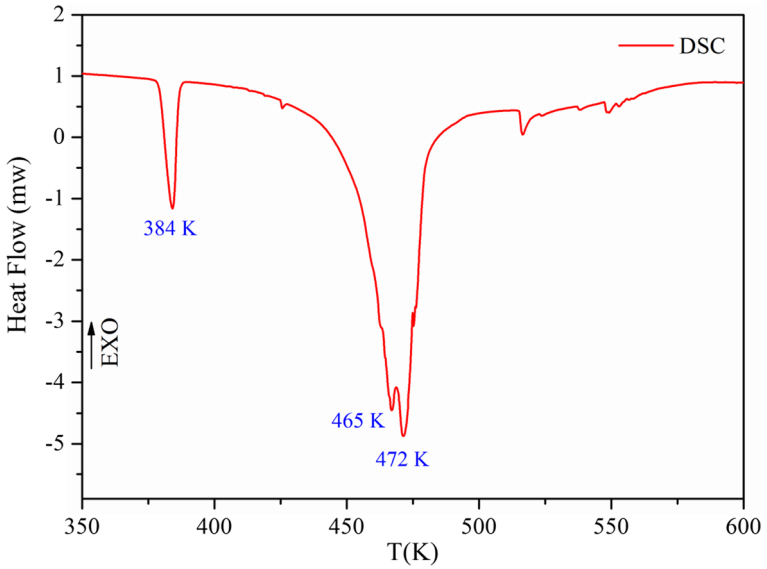

Fig. 6 Differential scanning calorimetry curve of $Tl_{0.92}(NH_4)_{0.08}(SO_4)_{0.65}(SeO_4)_{0.35}Te(OH)_6$

of 5 K min^{-1}. As shown in Fig. 6, the DSC curve for the TlNSSeTe crystal reveals three endothermic peaks at 384, 465 and 472 K.

The calculated transition enthalpy, for the first transition at $T_1 = 384$ K, is $\Delta H_1 = 17.51$ Jg $^{-1}$.

Yet, the second and the third peaks are stacked with other peaks. Hence, the enthalpy corresponding to the sum of these peaks is $\Delta H_2 = 112.93$ Jg $^{-1}$. As compared to other similar compounds, the first transition of the title compound at 384 K can be assigned to the structural phase transition, which allows a non-centrosymmetric phase at an elevated temperature [11, 22, 34]. Otherwise, the second phase, which occurs at 465 K, can be attributed to a ferroparaelectric phase transition. The latter is congruent with those found for other tellurate compounds described in the literature [11, 32–34]. The third endothermic peak, which takes place at 472 K, refers to a phase transition of protonic conduction due to the breaking of O–H…O hydrogen bonds that connect TeO_6 to S/SeO_4 [4, 15, 32–34, 37].

In previous works, after the thermal analysis, the material conserves its solid state, which proves that the melting temperature has not been reached [18, 34].

Thermogravimetric (TG) and differential thermal analysis (DTA)

To characterize the new material more fully in terms of thermal stability, such a structural arrangement is recorded in the new TlNSSeTe structure, which is described by the presence of three independent and different anions (SO_4^{2-}, SeO_4^{2-} and TeO_6^{6-} groups) associated by O–H…O and N–H…O hydrogen bonds. In order to get further data about these phase transitions, we performed thermodifferential and thermogravimetric measurements from 300 to 1100 K.

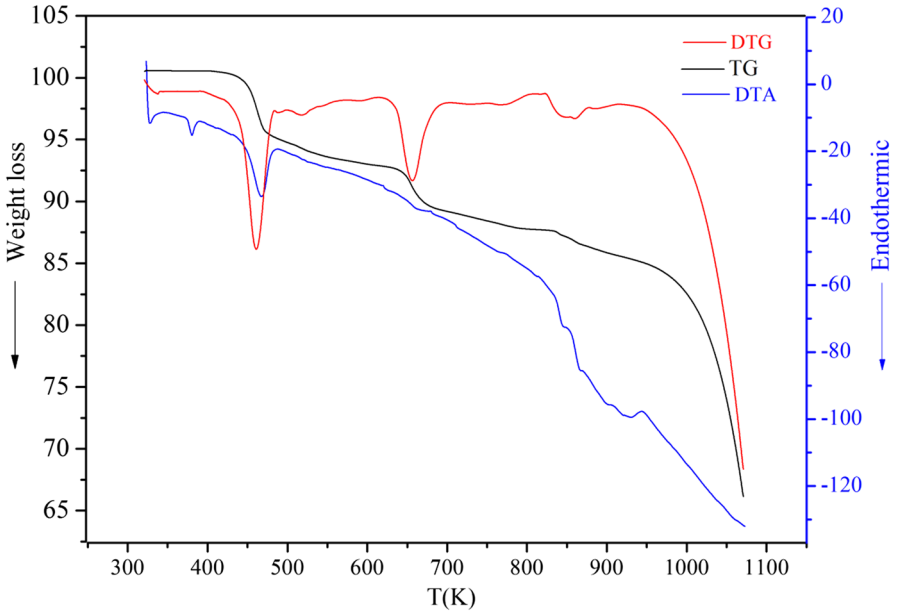

Fig. 7 TG–DTG–DTA curves of $Tl_{0.92}(NH_4)_{0.08}(SO_4)_{0.65}(SeO_4)_{0.35}.Te(OH)_6$ material

The superposition of TG/DTG, DTA curves presented in Fig. 7 prove that the first peak observed in DTA at $T_1 = 380$ K does not induce a weight loss, which proves that the (TlNSSeTe) undergoes structural changes over the same temperature. This result is in total agreement with the previous DSC calorimetric study, which revealed an endothermic peak at 386 K. In addition, TG/DTG curves of TlNSSeTe revealed total mass losses of 14.76% starting from 418 up to 1050 K. As shown in Fig. 7, TG curves of our compound contain three significant weight losses.

The first weight loss of 7.43% from 418 to 491 K (which reaches its maximum velocity at 465 K), is related to endothermic peaks at 467 and 464 K on DTA and DSC curves, respectively. Basically, this mass loss accounts for the dehydration process. For this reason, we deduce that all of the mass loss is concomitant with the decomposition of telluric acid $Te(OH)_6$, which corresponds to the loss of three water molecules. This suggests that this decomposition is expressed as follows [38]:

$$Te(OH)_6 \rightarrow TeO_3 + 3H_2O \tag{2}$$

Comparing the obtained results with the already performed studies, we infer that the decomposition of telluric acid is not a single-step process [34].

$$Te(OH)_6 \rightarrow H_2TeO_4 + 2H_2O \tag{3}$$

Therefore, the decomposition of the our material can be indicated as follows:

$$\begin{aligned} &Tl_{0.92}(NH_4)_{0.08}(SO_4)_{0.65}(SeO_4)_{0.35}Te(OH)_6 \\ &\rightarrow\ Tl_{0.92}(NH_4)_{0.08}(SO_4)_{0.65}(SeO_4)_{0.35}H_2TeO_4 + 2H_2O \end{aligned} \tag{4}$$

Furthermore, the orthotelluric acid H_2TeO_4 begins to decompose between 492 and 720 K, with water liberation, as described by Faby et al. [38].

$$H_2TeO_4 \rightarrow TeO_3 + H_2O \quad (5)$$

This phenomenon is demonstrated in the decomposition of telluric acid and some additional compounds, such as TlKSSeTe [11, 34].

The second mass loss of 18.2%, which coincides well with the theoretical value 19%, starts at 500 and finishes at 638 K (which reaches its maximum velocity at 613 K). It is related to endothermic peak on the DTA at 661 K. It is reported in literature that in certain compounds, this loss is ascribed to the ammonia molecule which loses 2 H^+ protons [33].

Consequently, the oxygen atom proves to form water molecules in the presence of two hydrogen atoms. As a matter of fact, at this temperature, a molecule of H_2O can be observed.

The third step is between 828 and 877 K, with total mass loss of 2.2% (which reaches its maximum velocity at 841 K), associated with endothermic peak at 891 K on the DTA corresponding to the loss of 0.5 O_2 molecule [11].

Similar to what is reported in literature, in the (TlNSSeTe) crystal, the telluric acid completes its decomposition at 877 K [33].

Vibrational spectroscopy study

In addition to the investigation of the solid state crystal structure, we also studied the vibrational properties of the new TlNSSeTe material (Figs. 8 and 9). We performed

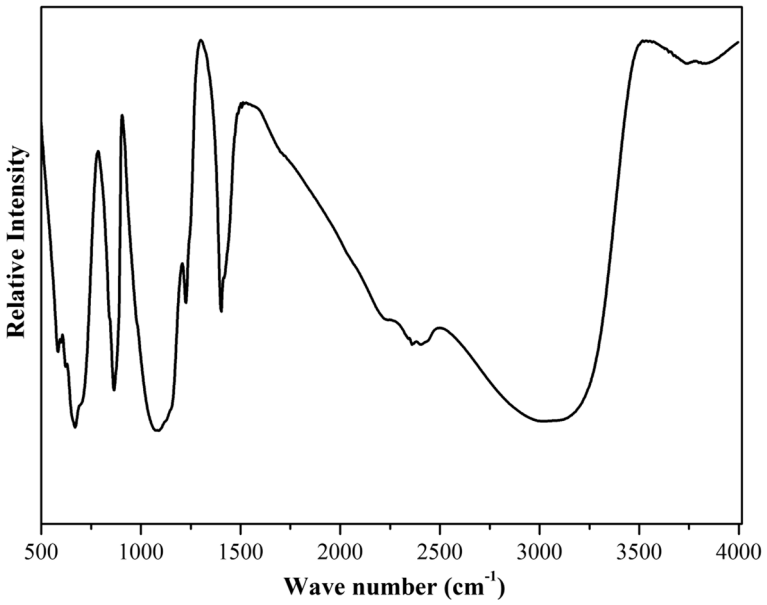

Fig. 8 IR spectrum at room temperature of the $Tl_{0.92}(NH_4)_{0.08}(SO_4)_{0.65}(SeO_4)_{0.35}Te(OH)_6$ compound

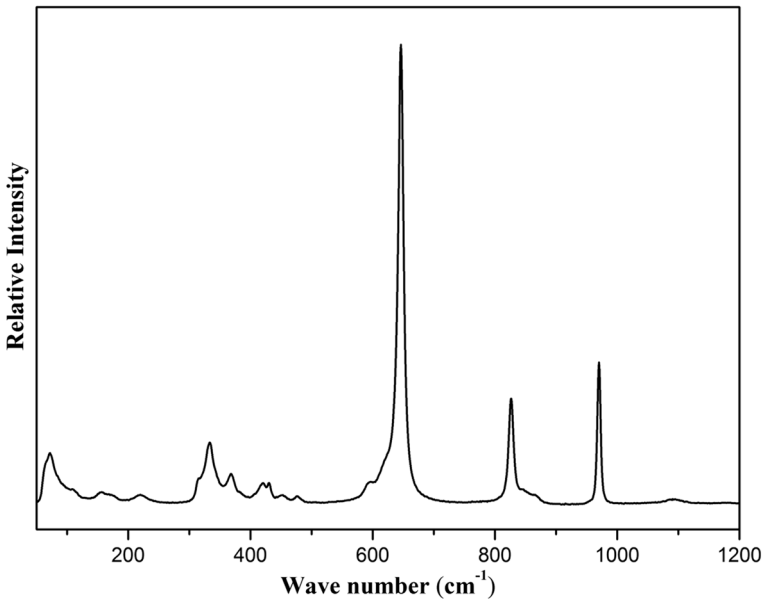

Fig. 9 Raman spectrum at room temperature of the $Tl_{0.92}(NH_4)_{0.08}(SO_4)_{0.65}(SeO_4)_{0.35}.Te(OH)_6$ compound

IR and Raman spectroscopic studies of this material to prove the presence of the three independent anion (TeO_6^{6-}, SO_4^{2-}, SeO_4^{2-}, Tl^+ and NH_4^+) groups and clarify the hydrogen bonds in their crystal lattice.

The study of IR and Raman spectra of this mixed compound at room temperature, which has been performed in the frequency ranges of 400–4000 cm^{-1} and 50–1200 cm^{-1}, is exhibited in Figs. 8 and 9. The observed bands and their attribution to different modes for the TlNSSeTe compound are displayed in Table 7.

Interpretation of the IR spectrum

The infrared spectroscopy is one of the basic physical methods of molecular structure investigation. At room temperature, the absorption of the TlNSSeTe compound presents a monoclinic symmetry with space group $P2_1/c$ in four formula units. The assignment of TeO_6, SO_4, SeO_4, NH_4 bands is performed by comparison with other similar materials (Table 7). For TlNSSeTe, the spectroscopically relevant unit is the TeO_6^{6-} anion. In fact, the ν_1 symmetric stretching of TeO_6 has been reported to appear in the IR spectrum at 646 cm^{-1} [12, 32, 34]; meanwhile, the intense peak detected at 592 cm^{-1} is related to the asymmetric stretching of $\nu_3(TeO_6)$ [11, 32, 33].

The comparison with previously published data [11] shows that all the vibrations belong to IR activity of the tetrahedral SeO_4 group in our compound, whereas only ν_4 is Raman active. The symmetric stretching vibration ν_1 of (SeO_4) appears in the spectra at 826 cm^{-1}. In addition, the line situated at 870 cm^{-1} is assigned to the asymmetric stretching (ν_3) mode of (SeO_4). $\nu_2(SeO_4)$ vibration appears in IR spectra at 471 cm^{-1}, as was already described for several selenate compounds [11, 34, 39].

Table 7 Observed IR and Raman frequencies (cm^{-1}) and band assignments for $Tl_{0.92}(NH_4)_{0.08}(SO_4)_{0.65}(SeO_4)_{0.35}Te(OH)_6$

IR	*I*	Raman	*I*	Assignment
3120	vs	–	–	$\nu_3(NH_4)$ and ν_{OH} of $Te(OH)_6$
2262	s	–	–	ν (OH) of hydrogen bond
2324	s	–	–	
2245	s	–	–	
1623	m	–	–	$\nu_2(NH_4)$
1418	m	–	–	$\nu_4(NH_4)$
1120	vw	1087	s	$\nu_3(SO_4)$
971	s	970	vs	$\nu_1(SO_4)$
870	vw	865	w	$\nu_3(SeO_4)$
826	vs	821	s	$\nu_1(SeO_4)$
646	m	646	vs	$\nu_1(TeO_6)$
–	–	628	s	$\nu_2(TeO_6)$ and $\nu_4(SO_4)$
592	w	591	m	$\nu_3(TeO_6)$
471	m	476	w	$\nu_2(SO_4)$
–	–	430	w	$\nu_2(SeO_4)$
–		420	w	$\nu_4(SeO_4)$
–	–	368	m	$\nu_5(TeO_6)$
–	–	332	s	$\nu_4(TeO_6)$
–	–	314	s	$\nu_2(SeO_4)$
–		219	w	$\nu_6(TeO_6)$
–		155	w	νOH…O
–		109	w	$T(NH_4^+)$
		71	m	TTl^+

Relative intensities: *vs* very strong, *s* strong, *m* medium, *w* weak, *vw* very weak

For SO_4 groups, the internal vibration of SO_4 tetrahedra has four vibrational modes, two stretching modes ν_1, ν_3 and two bending modes ν_2 and ν_4 of a regular tetrahedron. The intense peak detected at 971 cm^{-1} is associated with the symmetric stretching (ν_1) mode of (SO_4) [11, 40, 41]. The asymmetric stretching vibration (ν_3) of (SO_4) tetrahedral (IR 1120 cm^{-1}) is known with other sulfates [33, 34, 40–43]. The ν_2 SO_4 vibration appears at 471 cm^{-1} [40, 43]. The stretching mode ν_4 SO_4 is active in Raman spectra [34].

The bands related to the vibration modes of NH_4^+ ions are more visible on the IR spectrum at frequencies upper to 1300 cm^{-1}. In fact, the weak line at 1418 cm^{-1} corresponds to ν_4 (NH_4^+) and the ν_2 (NH_4^+) appears at 1623 cm^{-1} [12]. The highest frequencies of the IR spectrum observed at 2245 cm^{-1}, 2324 cm^{-1} and 2362 cm^{-1} may be attributed to the symmetric and asymmetric stretching vibrations of the O–H…O groups of the hydrogen bond [12, 33].

Finally, the strong band observed at around 3120 cm^{-1} in IR spectra, can be assigned to ν_3 (NH_4^+) and the O–H stretching vibration was already described for

several tellurate compounds [11, 33, 34]. This IR spectrum is congruent with the results of X-ray structural analyses.

Interpretation of Raman spectrum

In the present study, a Raman spectroscopic measurement of this new material was determined and analyzed. The Raman spectrum of the material TlNSSeTe exhibits internal and external vibrations. Based on preceding works focusing on similar materials containing TeO_6^{6-}, SO_4^{2-} and SeO_4^{2-} ions, we suggest certain assignments of the observed bands [11, 34].

The stretching and bending vibrations for materials containing TeO_6 group generally take place in regions 550–750 and 350–450 cm^{-1}, respectively [11, 17, 34]. At room temperature, the Raman spectrum of our mixed compound is highly resolved, which proves the presence of the polar phase. In fact, the intense peak around 646 cm^{-1} is attributed to the symmetric stretching $\nu_1(TeO_6)$ [11, 34–36], while the peak appearing at 628 cm^{-1} is assigned to the ν_2 vibration of TeO_6. Moreover, the two vibration modes $\nu_3(TeO_6)$ [11, 12, 32–34] and $\nu_4(TeO_6)$ take place at respectively 591 cm^{-1} and 314 cm^{-1}. The band observed at 368 cm^{-1} corresponds to $\nu_5(TeO_6)$ [33, 34]. However, $\nu_6(TeO_6)$ vibration appearing in the spectra at 219 cm^{-1} is in agreement with Wilson's rule $\nu_5(TeO_6) = \sqrt{2}\,\nu_6(TeO_6)$ [34].

In addition, the peak detected at 821 cm^{-1} is assigned to ν_1 (SeO_4) tetrahedral groups. The $\nu_4(SeO_4)$ [11, 34] vibration appears in this spectra at 420 cm^{-1}. The band observed at 865 cm^{-1} corresponds to ν_3 (SeO_4), and is in excellent agreement with published results for TlKSSeTe [11]. Only ν_2 is active in IR spectra.

According to Raman spectra, the strongest symmetric stretching mode ν_1 (SO_4) tetrahedral groups take place at 970 cm^{-1} [17, 33, 34], but the asymmetric mode ν_3 (SO_4) (Raman 1087 cm^{-1}) is found at lower values [34]. Two modes observed at 476, 628 cm^{-1} involve both ν_2 (SO_4) and ν_4 (SO_4) [11, 33, 34, 43].

Below 200 cm^{-1}, the low-frequency includes the translation modes of Tl^+ cations located at 71 cm^{-1} [11]. The very weak band detected at 109 cm^{-1} is assigned to the lattice modes. This result is compatible to other results [12]. The peak appearing at 155 cm^{-1} can be assigned to the vibration and translation modes of (S/SeO_4^{2-} and TeO_6^{6-}) anions [11, 34]. These data are in good agreement with the Raman data of thallium rubidium sulfate selenate tellurate [11].

Conclusion

This work focuses on the synthesis, X-ray characterization, thermal features and vibrational investigation of a new mixed thallium ammonium sulfate selenate tellurate, $Tl_{0.92}(NH_4)_{0.08}(SO_4)_{0.65}(SeO_4)_{0.35}.Te(OH)_6$. The structure is determined by a single crystal X-ray analysis, showing that this new solid solution crystallizes in a monoclinic system ($P2_1/c$ space group) at room temperature.

The structure is built up of planes of TeO_6 octahedra and pure S/SeO_4 tetrahedra. The Tl^+/NH_4^+ cations are interpolated between these types of polyhedra. Two types

of hydrogen bonds O–H…O and N–H…O maintained the stability of the (TlNS-SeTe) structure.

In addition, the DSC and DTA analyses reveal three phase transitions, the first is detected at 384 K, favoring the structural phase, while the second and third ones detected at 465 K and 472 K are assigned to the ferroelectricity and the superprotonic conduction, respectively. The TG curve indicates that no mass loss is detected from room temperature up to 418 K.

Basically, the IR and Raman spectra, acquired at room temperature, prove the presence and the independence of different anions (TeO_6^{6-}, SO_4^{2-}, SeO_4^{2-}, Tl^+ and NH_4^+) associated with two types of hydrogen bonds that can be the source of interesting physical characteristics.

Acknowledgements This work is supported by the Ministry of Higher Education and Research of Tunisia. Authors would like to thank Pr. Kamel Maaloul from the English Language Unit at the Faculty of Sciences of Sfax for accepting to proofread and polish the language of this paper.

References

1. J. Lin, K. Diefenbach, J.N. Cross, J.M. Babo, T.E. Albrecht-Schmitt, Inorg. Chem. **52**, 13278 (2013)
2. J. Lin, K. Diefenbach, N. Kikugawa, R.E. Baumbach, T.E. Albrecht-Schmitt, Inorg. Chem. **53**, 8555 (2014)
3. J. Lin, J.N. Cross, J. Diwu, N.A. Meredith, T.E. Albrecht-Schmitt, Inorg. Chem. **52**, 4277 (2013)
4. J. Lin, J.N. Cross, J. Diwu, M.J. Polinski, E.M. Villa, T.E. Albrecht-Schmitt, Inorg. Chem. **51**, 11949 (2012)
5. J. Lin, J.N. Cross, J. Diwu, E.M. Villa, T.E. Albrecht-Schmitt, Inorg. Chem. **51**, 10083 (2012)
6. Y.Y. Tang, Z.Z. He, W.B. Guo, S.Y. Zhang, M. Yang, Inorg. Chem. **53**, 5862 (2014)
7. J. Lin, P. Chai, K. Diefenbach, M. Shatruk, T.E. Albrecht-Schmitt, Chem. Mater. **26**, 2187 (2014)
8. H. Litaiem, M. Dammak, T. Mhiri, A. Cousson, J. Alloys Compd. **396**, 34 (2005)
9. L. Ktari, M. Dammak, A. Hadrich, A. Cousson, M. Nierlich, F. Romain, T. Mhiri, Solid State Sci. **6**, 1393 (2004)
10. L. Ktari, M. Dammak, A. Madani, T. Mhiri, Solid State Ion. **145**, 225 (2001)
11. A. Elferjani, S. Garcia-Granda, M. Dammak, J. Alloys Compd. **749**, 448 (2018)
12. K. Ghorbel, H. Litaiem, L. Ktari, S. Garcia-Granda, M. Dammak, Chem. Res. Chin. Univ. **32**, 902 (2016)
13. H. Khemakhem, Ferroelectrics **234**, 47 (1999)
14. R. Zilber, A. Durif, M.T. Averbuch-Pouchot, Acta Cryst. B **36**, 2743 (1980)
15. R. Zilber, A. Durif, M.T. Averbuch-Pouchot, Acta Cryst. B **37**, 650 (1981)
16. R. Zilber, A. Durif, M.T. Averbuch-Pouchot, Acta Cryst. B **38**, 1554 (1982)
17. M. Dammak, H. Khemakhem, T. Mhiri, A.W. Kolsi, A. Daoud, J. Alloys Compd. **280**, 107 (1998)
18. M. Dammak, H. Khemakhem, T. Mhiri, J. Phys. Chem. Solids **62**, 2069 (2001)
19. L. Ktari, M. Dammak, A.W. Kolsi, A. Cousson, J. Alloys Compd. **476**, 54 (2009)
20. M. Dammak, L. Ktari, A. Cousson, T. Mhiri, J. Solid State Chem. **178**, 2109 (2005)
21. L. Ktari, M. Dammak, T. Mhiri, J.M. Savariault, J. Solid State Chem. **16**, 1 (2000)
22. M. Abdelhedi, M. Dammak, A.W. Kolsi, A. Cousson, Anal. Sci. X-ray Struct. Anal. Online **24**, 93 (2008)
23. M. Abdelhedi, L. Ktari, M. Dammak, A. Cousson, A.W. Kolsi, J. Alloys Compd. **460**, 147 (2008)
24. M. Abdelhedi, M. Dammak, A. Cousson, A.W. Kolsi, J. Alloys Compd. **398**, 55 (2005)
25. M. Dammak, A. Hadrich, T. Mhiri, J. Alloys Compd. **428**, 8 (2007)
26. L. Ktari, M. Dammak, T. Mhiri, A.W. Kolsi, Phys. Procedia. **2**, 729 (2009)
27. Nonius, in: B.V. Nonius (Ed.), Kappa CCD Sever Software, Delft, The Netherlands, 1999
28. APEX2 version 1. 0–8, Bruker AXS, Madison, WI, 2003

29. D.J. Watkin, C.K. Prout, J.R. Carruthers, P.W. Betteridge, R.I. Cooper, *CRYSTALS Issue 11* (Chemical Crystallography Laboratory, Oxford, UK, 2001)
30. K. Brandenburg, M. Berndt, DIAMOND Version 2.1.b, Crystal Impact, Gb R, (Bonn, Germany 1999)
31. Y.Y. Tang, W.B. Guo, S.Y. Zhang, M. Yang, Z.Z. He, Cryst. Growth Des. **14**, 5206 (2014)
32. H. Frikha, M. Abdelhedi, M. Dammak, S. Garcia-Granda, J. Saudi Chem. Soc. **21**, 324 (2017)
33. K. Ghorbel, H. Litaiem, L. Ktari, S. Garcia-Granda, M. Dammak, J. Mol. Struct. **1079**, 225 (2015)
34. A. Elferjani, M. Abdelhedi, M. Dammak, A.W. Kolsi, J. Appl. Phys. A. **122**, 742 (2016)
35. K. Ghorbel, H. Litaiem, L. Ktari, S. Garcia-Granda, M. Dammak, Ionics **22**, 251 (2016)
36. A. Novak, *Hydrogen Bonding in Solids*, vol. 18 (Spring, Berlin, 1974), p. 177
37. M. Djemel, M. Abdelhedi, L. Ktari, M. Dammak, J. Mol. Struct. **1033**, 84 (2013)
38. J. Faby, J. Loub, L. Feltl, J. Therm. Anal. **24**, 95 (1982)
39. R. Ayadi, J. Lhoste, I. Ledoux-Rak, T. Mhiri, M. Boujelbene, J. Saudi Chem. Soc. **21**, 869 (2017)
40. Y.Y. Tang, M. Cui, W.B. Guo, S.Y. Zhang, M. Yang, Z.Z. He, Cryst. Growth Des. **15**, 2742 (2015)
41. B. Yotnoi, A. Rujiwatra, M.L.P. Reddy, D. Sarma, S. Natarajan, Cryst. Growth Des. **11**, 1347 (2011)
42. K. Jaouadi, N. Zouari, T. Mhiri, Phase Transit. **90**, 143 (2017)
43. N. Nouiri, K. Jaouadi, T. Mhiri, N. Zouari, Ionics **22**, 1611 (2016)